Received: 12 February 2019 | Revised: 27 June 2019 | Accepted: 22 July 2019

DOI: 10.1002/ese3.430

RESEARCH ARTICLE

Energy Science & Engineering Open Access

Experimental study of the effects of turbine solidity, blade profile, pitch angle, surface roughness, and aspect ratio on the H-Darrieus wind turbine self-starting and overall performance

Longhuan Du[1] | **Grant Ingram**[2] | **Robert G. Dominy**[3]

[1]College of Architecture and Environment, Sichuan University, Chengdu, China

[2]Department of Engineering, Durham University, Durham, UK

[3]Faculty of Engineering and Environment, Department of Mechanical & Construction Engineering, Northumbria University, Newcastle, UK

Correspondence
Longhuan Du, College of Architecture and Environment, Sichuan University, Chengdu, China.
Email: longhuan_du@163.com

Funding information
Sichuan Science and Technology Program, Grant/Award Number: 2018JY0595

Abstract

New and comprehensive time-accurate, experimental data from an H-Darrieus wind turbine are presented to further develop our understanding of the performance of these turbines with a particular focus on self-starting. The impact of turbine solidity, blade profile, surface roughness, pitch angle, and aspect ratio on the turbine's performance is investigated, parameters that are thought to be critical for small-scale VAWT operation, particularly when operating in the built environment. It is demonstrated clearly that high turbine solidity ($\sigma \geq 0.81$) is beneficial for turbine self-starting and that the selection of a thick, symmetrical aerofoil set at a low, negative pitch angle ($\beta \geq -2°$) is better than a cambered foil. Increased blade surface roughness is also shown to improve a turbine's self-starting capability at low tip speed ratios and with high turbine solidity and the associated flow physics are discussed. Finally, it was confirmed that blade span has a significant impact on turbine starting. This paper contributes to the understanding of the turbine characteristics during the starting period and provides clear guidance and validation cases for future design and research in order to promote and justify the wider application of this wind turbine configuration.

KEYWORDS

design parameters, H-Darrieus, self-starting, turbine performance, vertical axis wind turbine

1 | INTRODUCTION

Small wind turbines are considered to be one of the most promising sources of clean electricity generation, particularly in the built environment. However, wind speeds in that environment are often low and unsteady with high levels of turbulence resulting in air flows that are characterized by rapid changes in speed and direction. Under these circumstances, vertical axis wind turbines (VAWTs) have been highlighted as more appropriate than the more commonly adopted horizontal axis wind turbines (HAWTs) thanks to several distinct advantages such as insensitivity to wind direction, ease of maintenance, simple blade shape, low cost, and low noise.[1-4]

The most significant challenges associated with employing these small machines are to make them self-starting (which is defined as the turbine's ability to reach its optimal power-extraction operation condition when driven only by the wind) and more efficient. However, VAWTs are often reported to suffer from low efficiency compared with HAWTs[5]

and the literature provides conflicting conclusions about the self-starting capability of an H-Darrieus wind turbine.[6]

Improvements in the understanding and prediction of VAWT performance have been achieved through the use of analytical models, CFD simulations, and through a small number of experimental measurements which have recently begun to use time-accurate techniques such as particle image velocimetry (PIV).

Examples of the recent development and application of analytical models include the work of Saeidi et al[7] and Svorcan et al[8] who evaluated the turbine aerodynamic design and economic aspects of a small-scale H-Darrieus wind turbine using the widely adopted double-multiple streamtube model (DMST). De Tavernier et al[9] applied a genetic algorithm to optimize airfoil shape considering a balance between the aerodynamic and structural performance. Dumitrescu[10] applied a vortex model to predict and analyze the low-frequency noise produced by H-Darrieus turbines, while a low-order aerodynamic model was applied by Hand and Cashman[11,12] to provide a low-cost computational design tool for studying H-Darrieus turbines to which it is well suited.

In terms of the CFD simulations, numerous aspects of VAWT performance have been studied. For example, Untaroiu et al[13] numerically studied the H-Darrieus turbine self-staring behavior but both 2D and 3D models failed to accurately predict the starting characteristic when compared to measured data. Arab et al[14] examined the turbine self-starting characteristics showing that the turbine's aerodynamic performance could be affected by the history of the flow field and that the rotor inertia would affect the turbine starting characteristics. Howell et al[15] demonstrated that although 3D models were in reasonably good agreement with experimental measurements, their 2D results significantly overestimated the performance coefficient. Danao et al[16] investigated unsteady wind effects on the performance of the turbine, and it was demonstrated that the overall turbine performance could be improved under certain unsteady conditions. Zhu et al[17] showed that the Gurney flap could improve turbine performance in a certain range of tip speed ratio and Rezaeiha et al[18] studied the impact of solidity and number of blades on the aerodynamic performance of H-Darrieus turbines. Meanwhile, the impact of a wider variety of operational parameters (λ, Reynolds number, and turbulence intensity) on the turbine performance was investigated by Rezaeiha et al[19] showing that turbine performance and wake are highly Re dependent up to $\mathrm{Re} = 4.2 \times 10^5$ and increasing λ increased the velocity deficit, wake expansion, and streamwise asymmetry in the wake. Wang et al[20,21] showed that blade leading edge serrations could improve turbine performance and their optimized turbine showed an 18.3% increase of power output. Zanforlin and Deluca[22] examined the effect of blade aspect ratio and Reynolds number on turbine power output. According to their results, both Reynolds number and tip losses would strongly influence the aerodynamic performance of the rotor and more advantages seemed to be achieved by limiting tip losses rather than increasing chord-based Reynolds number.

With regard to experimental measurements, Mazarbhuiya et al[23] investigated turbine performance using different asymmetric blades with a focus on the influence of blade thickness. It was demonstrated that thicker blades could improve the turbine torque and power. Bianchini et al[24] studied both the global turbine performance and the wake structure using a combination of a torque meter, wind speed, and hot wire anemometer. The velocity values measured experimentally in the wake compared well with their CFD predictions and the experiment provides a useful source of CFD validation data. Weber et al[25] studied turbine noise in the wind tunnel with a 1/2-inch free-field microphones. They showed that the main sources of the H-Darrieus sound pressure field were the separation-stall and the blade vortex interaction. Battisti et al[26] critically reviewed the main wind tunnel campaigns conducted on VAWTs during the last 15 years and the aerodynamic performance of two different rotor architectures (H-shaped and troposkien) was also investigated. Miller et al[27] examined the power coefficient of a model turbine at high Reynolds number but it should be noted that this exceeds the Re to which the full-scale turbine is exposed in the field. Parker and Leftwich[28] examined the effect of tip speed ratio by using the PIV technique and a symmetric wake behind the turbine is revealed. Tescione et al[29] analyzed the wake flow by using the stereoscopic particle image velocimetry (SPIV), revealing the evolution of the blade's tip vortices. Rolin and Porte-Agel[30] also studied the turbine wake using SPIV, and the presence of two pairs of counter-rotating vortices at the edges of the wake was observed. Buchner et al[31] compared their SST simulation results of blade dynamic stall with the SPIV measurement, which showed good agreement.

It is noted that only limited studies for investigating the turbine self-starting behavior are available. In particular, high-quality experimental data illustrating the performance trends associated with parametric design changes remain scarce and very few studies have been performed at the low tip speed ratios (λ) which are critical to the understanding of turbine starting characteristics.

To develop our understanding of turbine starting characteristics, a 3-bladed, H-Darrieus turbine was chosen in this study since it is well documented that 3-bladed designs have good self-starting capability and that they have been reported to be able to self-start irrespective of their starting position.[6,32] Three turbine solidities from low ($\sigma = 0.67$), middle ($\sigma = 0.81$), and high ($\sigma = 1.0$) were examined with three typical blade profiles. Small negative pitch angles ($\beta = -2°$ and $\beta \geq -4°$) were also investigated in order to understand the impact on turbine self-starting. The blade aspect ratio was modified by changing the blade span and two aspect ratios, $AR = 7$ and $AR = 6$, were selected to present here as they

straddle a distinct change in starting characteristic. Finally, blade surface roughness effects on turbine performance were also examined in this study.

The overall aim of this paper is to:

- Investigate the influence of design features including turbine solidity, blade profile, blade surface roughness, pitch angle, and aspect ratio on turbine performance especially at low tip speed ratios in order to fill a gap of the understanding of the turbine starting behavior.
- Provide high-quality and comprehensive experimental data including time-accurate self-starting data and overall $C_p \sim \lambda$ measurements to expand the currently small base of experimental data for future numerical validation.
- Present clear guidelines for the design of small-scale H-Darrieus wind turbines that can self-start in the low wind, built environment and to justify and promote the application of the turbine.

2 | EXPERIMENTAL CONFIGURATION

2.1 | The turbine blades

A review of published literature identified three typical and widely used blade profiles for small-scale VAWTs that might be suitable for this study. The blades of interest were as follows:

- NACA0021: The symmetric NACA00xx series has a relatively large thickness and is the most widely used family of profiles for VAWT applications. They have been shown to demonstrate relatively good turbine performance.[16,33,34]
- The DU06W200 profile was designed specifically for VAWT application having 20% thickness with 0.8% camber. This blade profile demonstrates better turbine performance especially during the starting period (low tip speed ratio) according to Claessens.[35]
- The NACA4415 profile, has a maximum camber of 4% and was suggested by Kirke and Lazauskas[36] as showing particularly good turbine self-starting capability.

Each blade was made from laser cut plywood laminates, each of 10 mm width, which were assembled to produce a complete blade. Two threaded bars were passed through the laminates so they could be assembled and clamped tightly together to form a continuous, uniform section blade. The chord length was $c = 100$ mm for all tested blades. In order to reduce their mass, the blades had central material removed but a significant wall thickness was maintained to retain strength and stiffness. This arrangement leads to the easy modification of blade span, S, by the addition or removal of laminates. Alternative blade spans were investigated in this study, and the test cases of $S = 600$ mm and $S = 700$ mm, corresponding to aspect ratios of $AR = 6$ and $AR = 7$, respectively, are presented here to demonstrate important changes in turbine performance.

Each blade was secured by two horizontal support arms. In order to connect the blades to the arms with sufficient accuracy and strength, two additional laminates made from perspex were used which included connection points for each blade as shown in Figure 1. Furthermore, by changing the relative location of the two attachment points on the perspex laminates, the blades could be fastened on the support arms at a preset pitch angle. Three pitch angles were investigated ($\beta = 0°$, $\beta = -2°$, and $\beta = -4°$) which were selected based upon evidence of improved performance from previous studies.[37] The definition of blade pitch (β) in this study is shown in Figure 2. Blade nose out is negative pitch ($-\beta$), and nose in is positive pitch (β).

2.2 | Testing arrangement

The tests were performed in the Durham University 2 m^2, 3/4 open-jet, open-return wind tunnel as shown in Figure 3. More details about this wind tunnel can be found in reference.[38] The turbine was centered in the jet in order to reduce shear layer and ground effects. The assembled turbine rotor was mounted on a $d = 15$ mm diameter central shaft which was supported by bearings at both ends to minimize vibration at high rotational speeds. The center shaft was aligned vertically using digital inclinometer with a resolution of 0.1°. The turbine's rotational speed and acceleration rate (or deceleration rate) were measured using an optical sensor and recorded

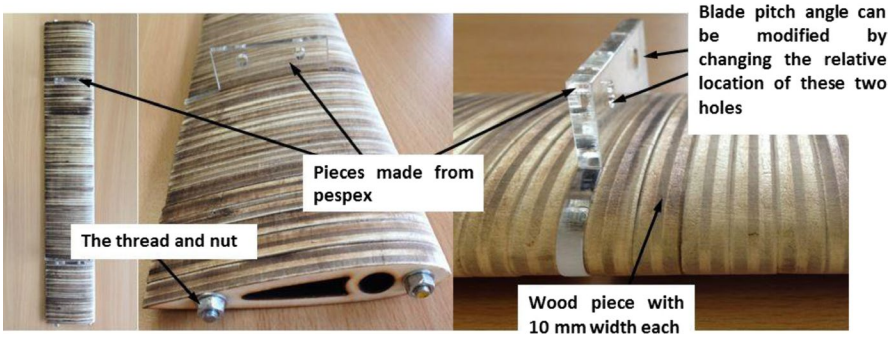

FIGURE 1 A typical blade showing clamping bars, wood laminates, and perspex mounting pieces

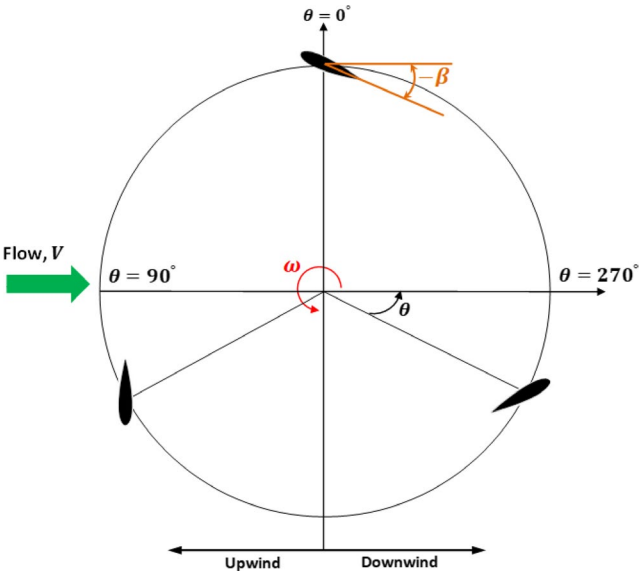

FIGURE 2 Definition of blade pitch angle, azimuth angle, upwind region, and downwind region

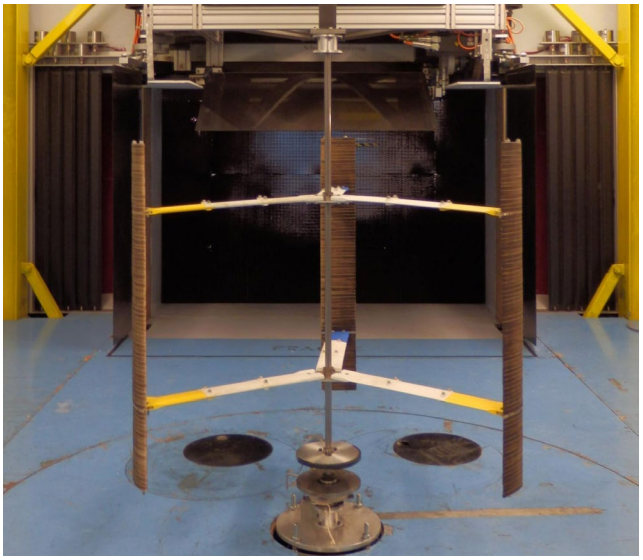

FIGURE 3 The three-bladed H-Darrieus wind turbine in the Durham 2 m^2, 3/4 open-jet, open-return wind tunnel

on a PC via a National Instruments USB-6218 ADC (details can be found in reference[38]).

Although the 3-bladed VAWT has the potential to start from all possible starting positions, it is known that the time to start can be affected by orientation[6] so for this study the same starting position was adopted for all tests for consistency. Furthermore, the concave side of the cambered blade was always set toward the central shaft.

In the present study, the turbine solidity was modified by changing the turbine radius, R, while keeping the number of blades, n, and blade chord length, c, the same. A schematic drawing of turbine configurations showing different solidities is presented in Figure 4.

2.3 | Blade surface roughness measurement

A turbine's blade surface roughness will be expected to increase during its lifetime through erosion or contamination, potentially affecting the machine's performance. In order to examine the effects of blade surface roughness on H-Darrieus wind turbine performance including its self-starting capability, blades with two different surface finishes were tested and compared. The original turbine blade was laser cut from high-grade plywood resulting in a relatively rough surface. To reduce the surface roughness, a new set of blades was manufactured and then coated with thin aluminum tape. The tape thickness was 0.03 mm which increased the blades thickness by less than 0.5% so the effect was ignored.

To quantify the roughness value, a ZETA-20 3-D profiler[39] was employed with a maximum resolution of 0.01 μm. For each surface finish, measurements were repeated using three sample pieces (30 mm × 30 mm) in order to calculate the averaged surface roughness value. The 3D color imaging is shown in Figure 5, and the test results are shown in Table 1. By examining the generally used parameters of arithmetic mean height, S_a, and root mean squared height, S_q, that represent an overall measurement of 3-D surface roughness, it can be clearly seen that the surface roughness of the wood sample was approximately 18 times larger than the one covered with aluminum tape, which ensured that the roughness comparison tests were representative and meaningful.

2.4 | Power and torque calculation

The method employed in this study to measure and calculate the blade torque (and power) followed the technique proposed by Edwards et al.[3] The force balance equation of the turbine system is determined by Equation (1). T_B is the net torque generated by all of the blades, T_{res} is the resistance torque generated by the whole system (excluding the blades), I_S is the whole system moment of inertia including blades, and this value is calculated from the mass and geometry of the rig, which is detailed in reference.[38] The angular acceleration, ξ, is calculated from two readings of rotational speed (ω_1 and ω_2) measured using the optical sensor. Knowing the time between the readings taken at t_1 and t_2, the acceleration (or deceleration) can be easily calculated by Equation (2) if the time interval is sufficiently short for the acceleration to be taken as linear.

$$T_B - T_{res} = I_s \xi \tag{1}$$

$$\xi = \frac{\omega_2 - \omega_1}{t_2 - t_1} \tag{2}$$

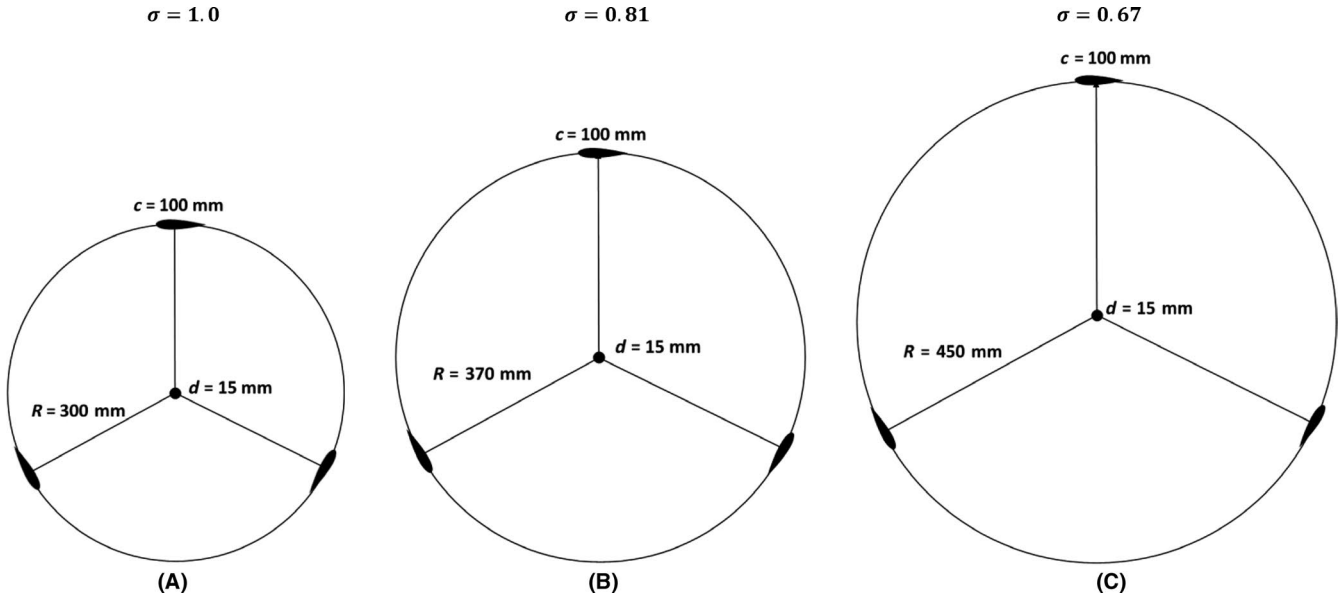

FIGURE 4 Schematic drawing of turbine configurations for different solidities

FIGURE 5 Local 3D color imaging from ZETA-20. A, Aluminum. B, Wood. Unit: μm

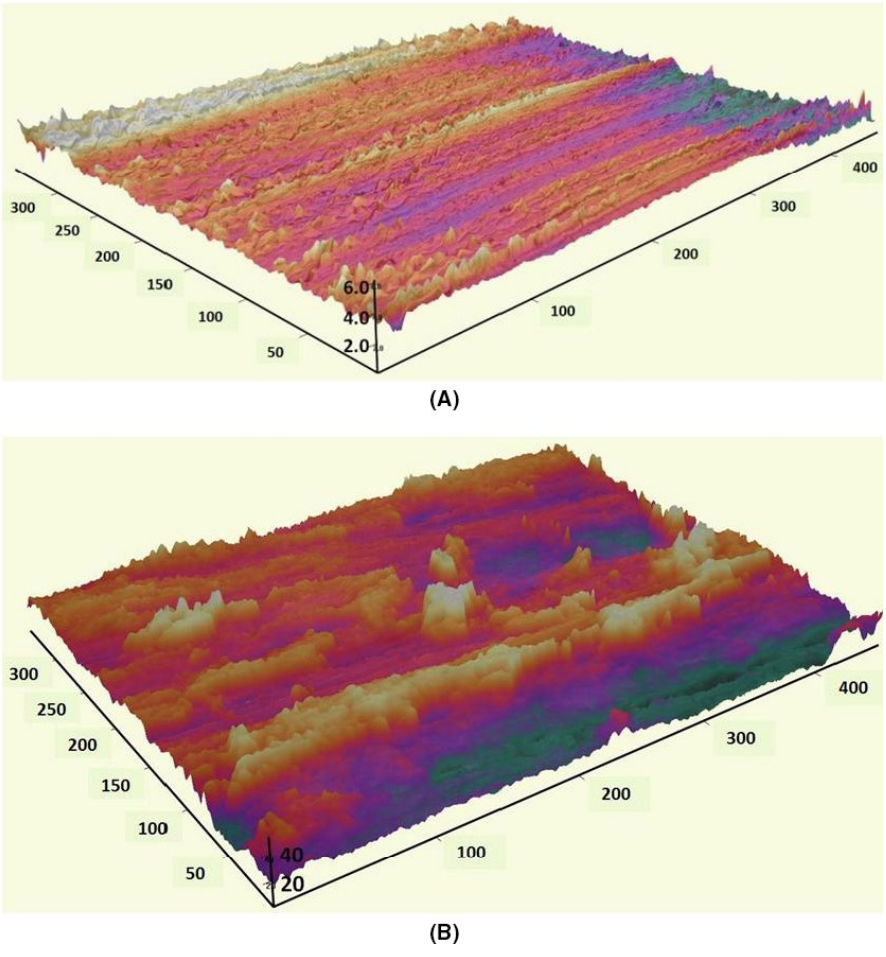

Spin-down tests were performed without the blades in order to calculate the whole turbine system resistance, T_{res}. The turbine was first driven by a motor up to a high rotational speed which exceeded the maximum speed for other tests. The motor was then disconnected from the turbine using a clutch mechanism, and the turbine was free to spin down. The turbine deceleration rate, ξ', was measured using the optical sensor, and T_{res} was then deduced from Equation (3). It must be noted that the moment of inertia of the rig without blades I_{rig} was calculated from the

TABLE 1 Measured surface roughness (mean value) of the wood sample and the sample covered with thin aluminum tape. Unit: μm

	S_a	S_q
Aluminum	0.22	0.28
Wood	4.02	5.02

component masses and geometry of the rig, which is detailed in reference.[3,38]

$$T_{\text{res}} = I_{\text{rig}}\left(\frac{\omega_2-\omega_1}{t_2-t_1}\right) = I_{\text{rig}}\xi' \tag{3}$$

Although the system resistance T_{res} varies continuously as the turbine spins down, a constant value was assumed across the time interval of $t_2 - t_1$. This assumption was justified by adopting a sensor sampling frequency of 200 Hz which was much higher than the maximum frequency that the turbine could reach (< 10 Hz). A series of readings could therefore be taken from peak rotational speed to zero, mapping out the $T_{\text{res}} - \omega$ curve. Moreover, the spin-down tests were repeated 6 times in order to calculate the averaged $T_{\text{res}} - \omega$ curve. Although the increased mass resulting from the addition of the blades might alter the bearing friction, the difference of T_{res} was negligible as also demonstrated by Edwards et al.[3]

Knowing the system resistance T_{res}, T_B can be calculated from a second test on the complete turbine, which is driven purely by the wind. The instantaneous turbine acceleration, ξ, is again recorded by the optical sensor.

Knowing the blade torque, T_B, the torque coefficient and power coefficient can then be determined from Equations (4) and (5), respectively.

$$C_T = T_B/0.5\rho ARV^2 \tag{4}$$

$$C_p = C_T\lambda \tag{5}$$

where ρ is air density, $A = 2R * S$ is the frontal area of the turbine, and V is the wind speed.

2.5 | Uncertainty

It should be noted that the calculation of moment of inertia of each turbine component is not exact but the maximum uncertainty of the calculated power coefficient, C_p, due to geometrical approximation was estimated to be less than 5%.[3,38] Since this geometrical approximation was used for all of the tests in this study, it should not affect the comparison between experimental results and the conclusions that may be drawn. Despite the simple blade construction method, the deviation of blade chord length and span of all the blades manufactured and used in this study was less than ±1 mm and ±5 mm, respectively, which resulted in less than ±1% uncertainty for the calculated turbine solidity and aspect ratio.

It is noted that the central shaft of the turbine could affect the turbine performance since the blade will interact with the wake shed from the shaft. According to Rezaeiha et al[40] the power loss of the turbine (reduction in C_p) increases asymptotically from 0% to 5.5% for shaft-to-turbine diameter ratio (δ) from 0% to 16%. The influence of shaft diameter becomes significant when $\delta > 4\%$. The diameter of the shaft in present study was 15 mm, which results in $\delta = 2.5\%$ for turbine radius, $R = 300$ mm, $\delta = 2.0\%$ for $R = 370$ mm, and $\delta = 1.7\%$ for $R = 450$ mm, respectively. Therefore, the impact of the central shaft on the reduction of C_p in the present study is estimated to be approximately $\Delta C_p \leq 1\%$.

3 | DATA POSTPROCESSING

3.1 | Turbine self-starting time-varying results

The turbine self-starting behavior was examined by measuring and recording the turbine's time-varying rotational speed. For each test configuration, the measurements were repeated 3 times to confirm good repeatability and low standard deviation as demonstrated by the example shown in Figure 6A,B. The beginning of each dataset was defined as when the turbine rotational speed became greater than 0.5 Hz. This format (averaged value with standard deviation of the mean) will be used throughout this paper to present the turbine time-varying, self-starting behavior.

3.2 | System resistance torque calculation

The system resistance torque, T_{res}, was measured by spin-down tests without blades for different turbine radii ($R = 300$ mm, $R = 370$ mm and $R = 450$ mm) at different free-stream wind speeds. For each configuration, 6 runs were performed in order to calculate the averaged $T_{\text{res}} - \omega$ curve based on Equation (3). Since I_{rig} is determined by the mass of the system components which is a constant, the relationship between T_{res} and ω was simplified into $\xi - \omega$. An example of the raw data is illustrated in Figure 7A.

Since T_{res} and ω have a second-order relationship, a quadratic polynomial fitting curve was produced based on the averaged value of the 6 runs as can be seen in Figure 7B. Finally, by considering the turbine inertia I_{rig} for each scenario, the corresponding $T_{\text{res}} - \omega$ curve can be produced as can be seen in Figure 7C. This $T_{\text{res}} - \omega$ fitted curve matches well with the averaged data throughout the rotational speed range, and therefore, it was used as a "look-up" table for

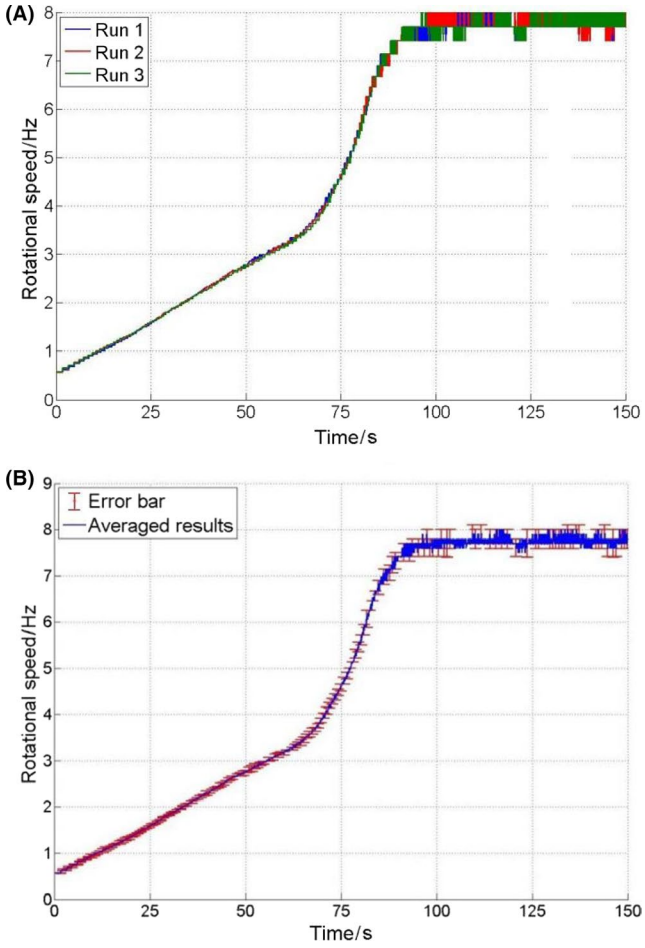

FIGURE 6 A, Example of three experimental measurements of turbine self-starting time-varying results. B, Averaged results with standard deviation of the mean (error bar)

calculating blade torque (T_B) which is detailed in the following section.

3.3 | Blade torque and power calculation

The instantaneous torque generated by the turbine blades (T_B) during self-starting was calculated based on Equations (1) and (2). The instantaneous turbine rotational speed was measured by the optical sensor, and the mean value from 3 runs was then used to calculate the instantaneous acceleration, ξ. Knowing the instantaneous system resistance, T_{res}, the relationship between blade torque and tip speed ratio ($T_B \sim \lambda$) can be easily established where the tip speed ratio is defined as $\lambda = \omega R/V = 2\pi fR/V$.

Examples are shown in Figure 8. The measured experimental results are presented with the standard error (standard deviation of the mean) showing the confidence range of the mean results from the 3 runs. Meanwhile, a fitted curve (smoothing spline) is added in order to show the overall trend of the experimental results against turbine tip speed ratio. Since under this testing condition, the turbine was purely driven by the wind, the self-starting process was highly unsteady, leading to the scatter in the $T_B \sim \lambda$ data. The fitted curve shows very good agreement with the experimental measurements at low tip speed ratios although some discrepancies exist between the fitted curve and the experimental results in the turbine's maximum torque region. However, even here the fitted curve still falls within the standard error range from the 3 runs for most of the measured points, providing reasonably good guidance. It should be noted that due to the limited number of runs, the calculated standard error might not represent the true value especially in the turbine's least stable operating region (high tip speed ratios). Therefore, these discrepancies between the fitted curve and the experimental data are simply due to the relatively small number of data sets from which the results were averaged.

Once the torque has been determined, the power coefficient can be calculated based on Equations (4) and (5). Examples are illustrated in Figure 9. The smoothing parameter, p, which was used to produce the smoothing spline was kept constant as $p = 0.995$ in this study in order to keep all the following results consistent (it should be noted that $p = 0$ produces a least-squares straight-line fit to the data while $p = 1$ produces a cubic spline interpolant).

It is noted that Rezaeiha et al[18] recently proposed that C_p was proportional to a new parameter "$\sigma\lambda^3$," which enables the maximum C_p to be almost independent of turbine geometrical and operational characteristics. However, their conclusions were drawn from a CFD study of just a single blade profile at one pitch angle so further analysis based on a much broader range of test conditions needs to be performed before that parameter can be used with confidence.

4 | RESULTS

4.1 | Turbine performance with different blade profiles and solidity

The three different blade profiles and other relevant parameters are summarized in Table 2. In this study, the turbine solidity is modified by changing the turbine radius, R, while keeping the blade chord length, c, and number of blades, n, constant. It should be noted that for most of the results shown in present study, the upstream wind speed is $V = 7$ m/s, resulting in a blade Reynolds number of $\text{Re} \approx 47\,000$ based on wind speed and blade chord.

The results for solidity, $\sigma = 1.0$, are illustrated in Figure 10. Time-varying data during the starting period is shown along with the corresponding $C_p \sim \lambda$ curves. The experimental measurements indicate the turbine with NACA0021 or DU06W200 blades can self-start at typical built environment wind speed of $V = 7$ m/s but the turbine with NACA4415 blades fails to self-start. Compared with the NACA0021 blade, as shown in Figure 10A, the recently proposed

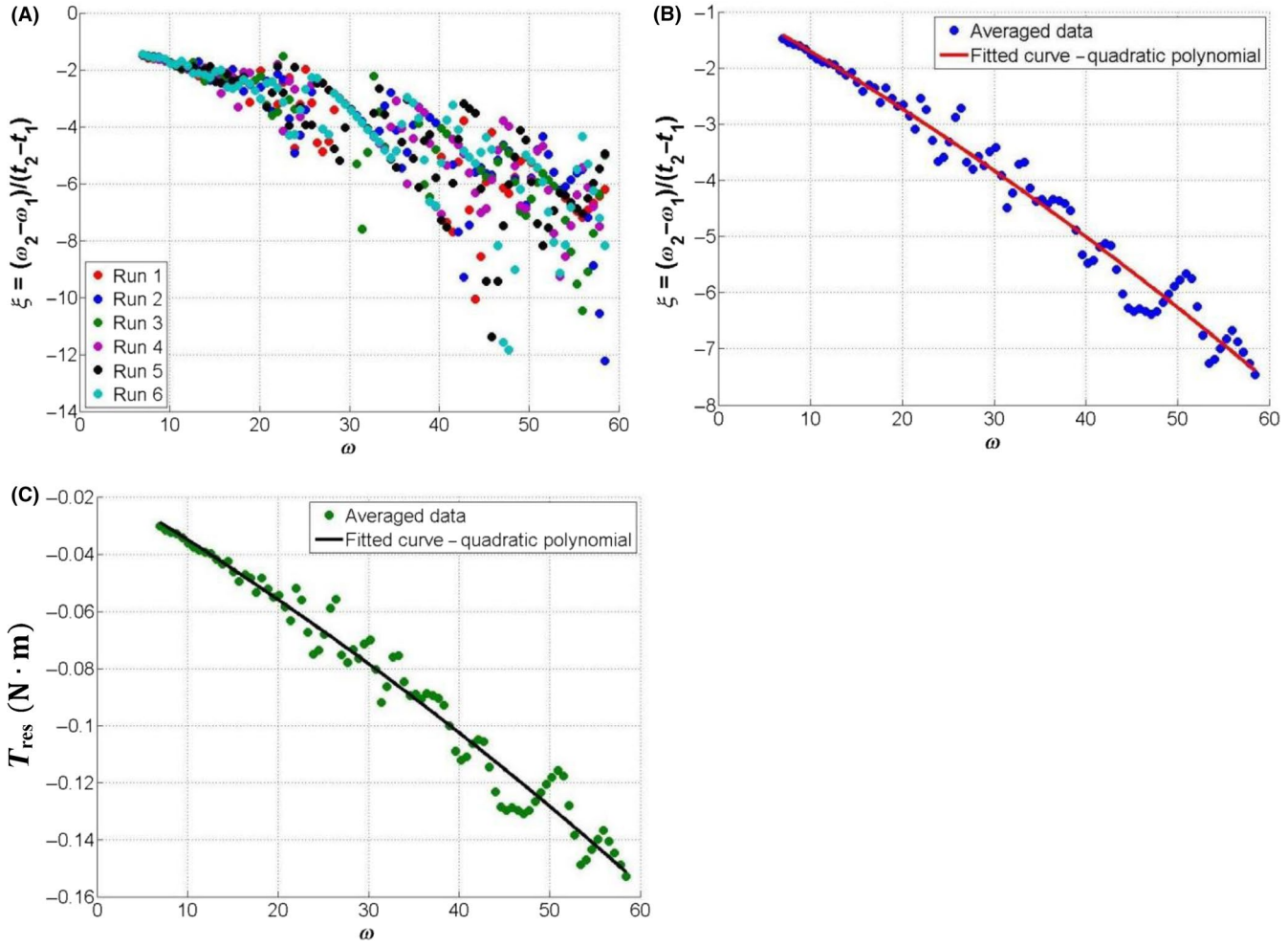

FIGURE 7 Example of measured turbine resistance. A, ξ-ω curve, raw data. B, ξ-ω curve, averaged data with quadratic polynomial fitted curve. C, Final T_{res}-ω curve, averaged data with quadratic polynomial fitted curve. $V = 6$ m/s, $R = 300$ mm

DU06W200 blade does not improve the turbine self-starting capability despite its lighter weight and lower inertia. Fitted with DU06W200 blades the turbine finally reaches maximum λ after approximately 90 seconds, while the turbine with NACA0021 profiles peaks 20 seconds earlier after about 70 seconds. The measured C_p from the DU06W200 is lower than that measured from the NACA0021 at low tip speed ratios, $\lambda < 1.2$, which is responsible for the longer self-starting time. With regard to the turbine's maximum power output, the DU06W200 peaks at the same tip speed ratio of $\lambda = 1.8$ as NACA0021 and it demonstrates a slightly higher power coefficient of approximately $C_p = 0.23$ as shown in Figure 10B.

Although the cambered NACA4415 blade performs better during the upwind sector as defined in Figure 2, the gain is more than offset by the loss in the downstream sector because of its unfavorable incidence angle. As a consequence, turbines with NACA4415 blades cannot pass the "dead band" region or plateau stage, where no positive torque can be produced by the blades as detailed in reference[32] and fail to self-start. The $C_p \sim \lambda$ curve for the NACA4415 blade is not plotted in Figure 10B since it provides no useful information. This is the opposite conclusion from that drawn by Kirke and Lazauskas[36] who claimed that a turbine with NACA4415 blades is able to self-start easily according to their analytical studies. It has been demonstrated[38,41] that mathematical models are highly sensitive to the quality of the input aerodynamic dataset which could have had an impact on their results.

Measurements were also performed at a turbine solidity $\sigma = 0.81$ and $\sigma = 0.67$. By decreasing turbine solidity, the turbine self-starting capability with any blade profile is reduced due to the reduced blockage effect and consequently reduced torque.[38] The turbine with DU06W200 and NACA0021 blades self-starts after about 150 seconds and 130 seconds respectively at $\sigma = 0.81$ (see Figure 11A). However, comparing with the situation at $\sigma = 1.0$ shown in Figure 10B, the turbine's maximum power coefficient is increased at $\sigma = 0.81$ but occurs at a higher tip speed ratio of $\lambda = 2.0$ (see Figure 11B). At a turbine solidity $\sigma = 0.67$, all of the turbines with wooden blades fail to self-start but the NACA0021 still demonstrates better performance than DU06W200 as shown in Figure 12 and it is possible that given long enough time the turbine would eventually start. The experimental measurements

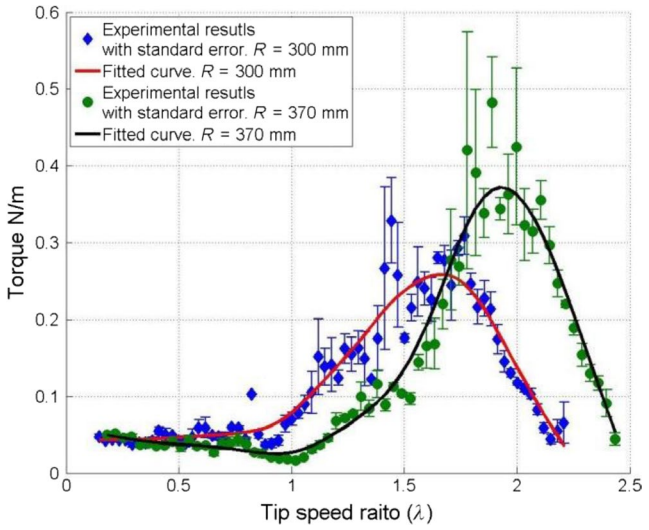

FIGURE 8 Examples of experimental measured torque (TB) with standard error and fitted curves

clearly indicate that faster turbine self-starting could be achieved by increasing turbine solidity but at the expense of lower peak power output.

4.2 | Turbine performance with different blade pitch angles

Three pitch angles were chosen to be examined experimentally: $\beta = 0°$, $\beta = -2°$ and $\beta = -4°$ for the NAC0021 profile. The blade span and chord length were kept the same as those shown in Table 2. Measurements were conducted at turbine solidities of $\sigma = 1.0$; $\sigma = 0.81$; and $\sigma = 0.67$.

The results at $\sigma = 1.0$ are presented in Figure 13. The time-varying data illustrate that the negatively pitched blades are able to improve turbine self-starting capability at low tip speed ratios as shown in Figure 13A. With its blades at $\beta = -2°$, the turbine acceleration profile is almost indistinguishable from the blade without pitch leading to peak velocity at the same tip speed ratio. At $\beta = -4°$, the acceleration is reduced and peak turbine speed is achieved about 30 seconds later. From the $C_p \sim \lambda$ curve shown in Figure 13B, it is observed that negatively pitched blades increase the turbine C_p at $\lambda < 0.9$. However, when $\lambda > 0.9$, both $\beta = -2°$ and $\beta = -4°$ blades produce less power than at $\beta = 0°$. Although $\beta = -2°$ shows similar peak power output with $\beta = 0°$, $\beta = -4°$ significantly degrades the turbine maximum performance.

According to previous studies and measurements,[42] it is demonstrated that the majority of the turbine torque is generated in the upwind region. Especially for the turbine at low λ as can be seen in Figure 14A, the blade experiences extremely high incidence angles and stalls for the majority of the revolution, producing limited positive torque and only in the upwind region. Therefore, at low λ, a negative pitched blade is able to delay the blade stall and help the blade to produce more power over a greater portion of the upwind region thus increasing its overall performance. With an increase of turbine rotational speed, the blade incidence range is significantly reduced and above a critical λ at which the blade will no longer experience stall at any point in its revolution. At relatively high λ, a negative pitch angle will decrease the blade incidence in the upwind region resulting in less torque being generated.

Although it is argued that this negative pitch angle will also increase the blade incidence in the downwind region, the majority of the driving torque is generated at the upwind region and the blade produces lower torque in the downwind region (see Figure 14B) leading to a decrease of net torque (or power) when integrated over a whole revolution. Therefore compared with $\beta = 0°$, the turbine with $\beta = -4°$ produces significantly lower power at $1.3 < \lambda < 2$ as shown in Figure 13B resulting in a much slower turbine acceleration at high λ and the turbine self-starts much later (see Figure 13A).

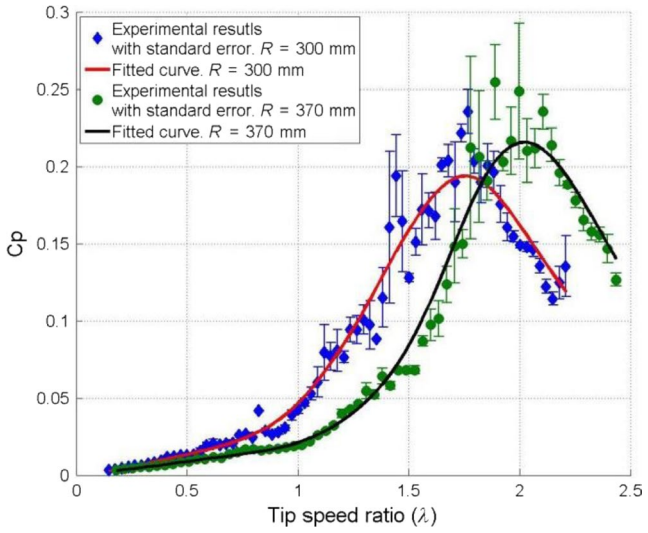

FIGURE 9 Examples of experimental measured power coefficient (C_p) with standard error and fitted curve

TABLE 2 Testing parameters for studies of turbine performance with different blade profiles

Blade profile	Solidity	*S*	*c*	*m*
NACA0021	$\sigma = 1.0$; $\sigma = 0.81$; $\sigma = 0.67$	700 mm	100 mm	460 g
DU06W200	$\sigma = 1.0$; $\sigma = 0.81$; $\sigma = 0.67$	700 mm	100 mm	414 g
NACA4415	$\sigma = 1.0$; $\sigma = 0.81$; $\sigma = 0.67$	700 mm	100 mm	388 g

Note: m is the mass of the blade.

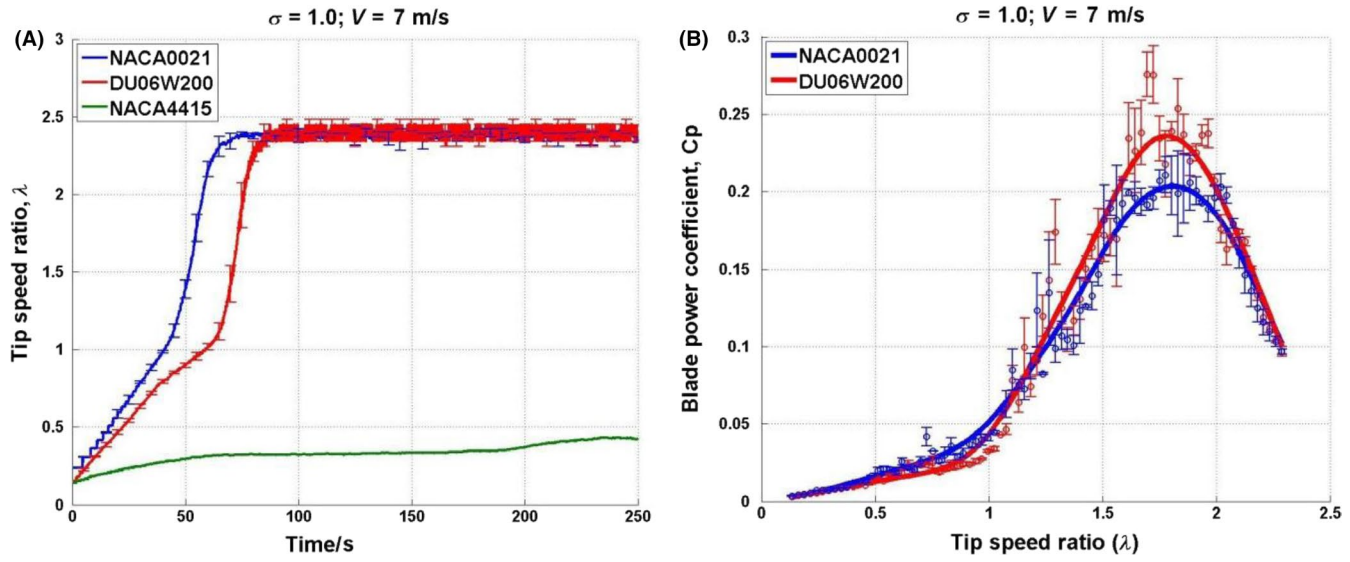

FIGURE 10 Turbine performance with three different blade profiles at $\sigma = 1.0$ and $V = 7$ m/s. A, Self-starting, time-varying results. B, $C_p \sim \lambda$ curve

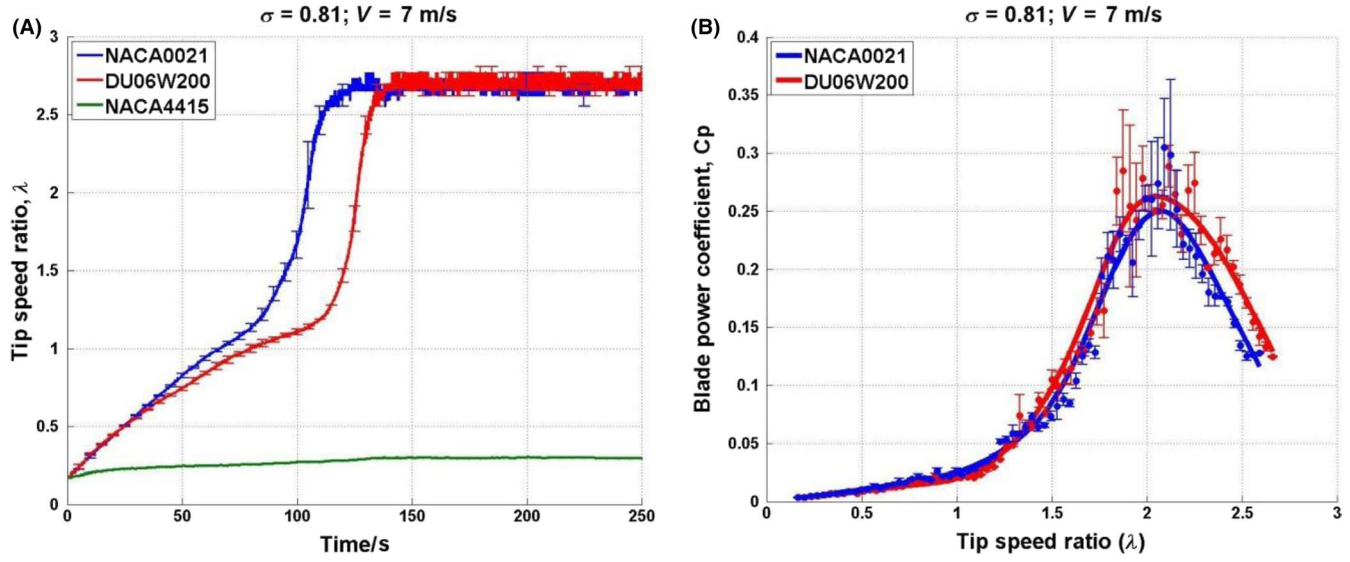

FIGURE 11 Turbine performance with three different blade profiles at $\sigma = 0.81$ and $V = 7$ m/s. A, Self-starting, time-varying results. B, $C_p \sim \lambda$ curve

At solidity, $\sigma = 0.81$, the advantages and disadvantages of negatively pitched blade become clearer. As can be seen in Figure 15, blades of $\beta = -2°$ and $\beta = -4°$ improve turbine performance only at low tip speed ratios ($\lambda < 1.3$), which leads to a faster initial acceleration. However a small, negative pitch angle ($\beta = -2°$) reduces the turbine acceleration rate when $\lambda > 1.3$ and too much negative pitch, $\beta = -4°$, completely prevents the turbine from self-starting.

At a solidity of $\sigma = 0.67$ (Figure 16), none of the turbines are able to self-start at this wind speed but the turbine with negatively pitched blades still clearly demonstrates a better initial turbine performance further supporting the above results and conclusions that slightly negatively pitched blades can improve the turbine performance during the first stage of start-up (low tip speed ratios).

4.3 | Turbine performance with different blade surface roughness

Experimental tests were performed using NACA0021 blades with two different surface finishes: wood and aluminum (Table 1). The blade span and chord length were kept the same as those shown in Table 2. Measurements were performed at turbine solidities of $\sigma = 1.0$; $\sigma = 0.81$, and $\sigma = 0.67$,

again with special attention paid to the turbine's critical self-starting behavior.

The results for a turbine at solidity, $\sigma = 1.0$, are illustrated in Figure 17. Both the rough blade and the smooth blade demonstrate almost identical starting behavior as shown in Figure 17A. However, in terms of the $C_p \sim \lambda$ performance, as shown in Figure 17B, the rough blade produces slightly more power than the smooth blade at low tip speed ratios (approximately $\lambda < 1.6$), but the smooth surface improves the turbine performance at high λ ($\lambda > 1.6$).

Similar results are observed for the turbine of $\sigma = 0.81$ as shown in Figure 18. Although the smooth surface shows slightly lower turbine performance at low λ, the turbine peak C_p and turbine power output at high tip speed ratio $\lambda \geq 2.2$ are both improved. These test results are consistent with previous experimental studies performed by Howell et al[15] and Ashwill.[43]

The improved performance from the rough blade at low tip speed ratios is explained by an earlier laminar to turbulent boundary layer transition. Therefore, a rough surface is able to delay the aerofoil stall and reduce the associated large drag force. However when the turbine rotational speed is increased, the incidence range is significantly reduced and the range of azimuth angles at which the aerofoil stalls are much reduced or even eliminated. Here, the increased skin friction drag resulting from the rough surface will outweigh the benefit from delayed stall resulting in lower performance than a smooth blade at high λ.

It is interesting to note that for turbine solidity, $\sigma = 0.67$, the experimental results shown in Figure 19 indicate the opposite conclusion from that drawn above. The smooth blade successfully enables the turbine to self-start while the rough blade turbine fails to self-start. It seems that at this low turbine solidity, the smooth blade actually improves the turbine performance at low λ.

One possible explanation for this phenomenon is that by further reducing the turbine solidity, the flow blockage is then reduced resulting in blade stall over a larger portion of azimuth angle in the upstream zone at low tip speed ratios. The benefit from the delayed stall of a rough surface becomes limited in this low solidity situation and cannot make up the loss from the increased skin friction drag. Therefore for a low solidity turbine blade experiencing stall over much of its revolution at low λ, a rough blade might not produce more net torque compared with a smooth blade. Nevertheless, it must be noted that the surface roughness effect on a blade's boundary layer is dependent on the blade Reynolds number, which varies with the rotational speed and azimuth angle.

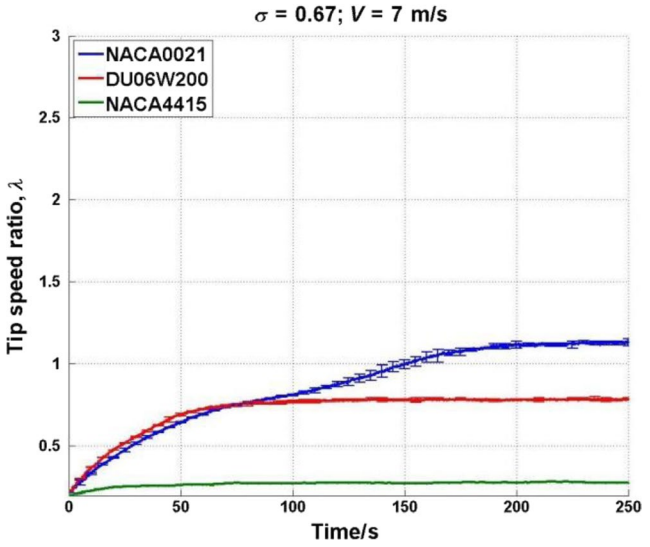

FIGURE 12 Turbine self-starting behavior with different blade profiles. $\sigma = 0.67$ and $V = 7$ m/s

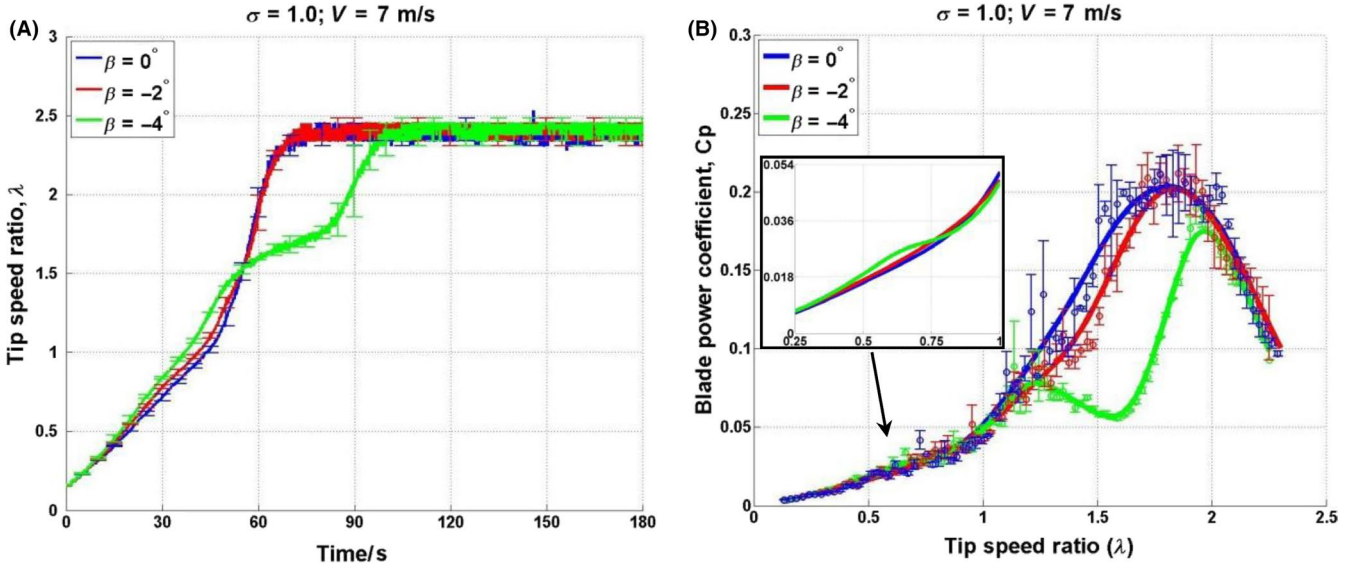

FIGURE 13 Blade pitch effects on turbine performance at $\sigma = 1.0$ and $V = 7$ m/s. A, Self-starting, time-varying results. B, $C_p \sim \lambda$ curve

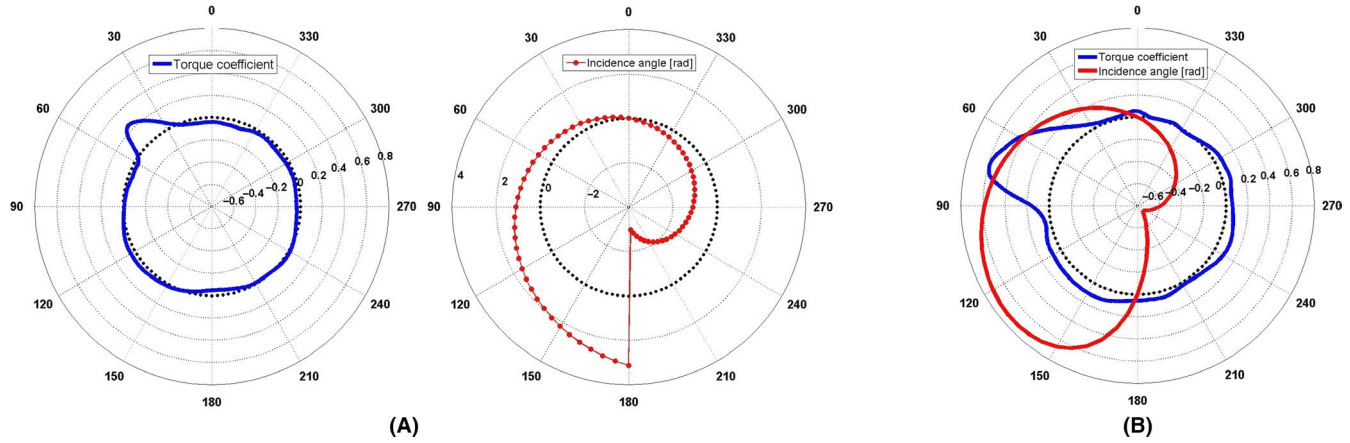

FIGURE 14 Three-bladed H-Darrieus wind turbine. A, $\lambda = 0.5$, torque coefficient and theoretical incidence angle. B, $\lambda = 1.5$, torque coefficient and theoretical incidence angle. $R = 300$ mm, $c = 100$ mm, $n = 3$, $\lambda = 0.5$, $V = 7$ m/s[42]

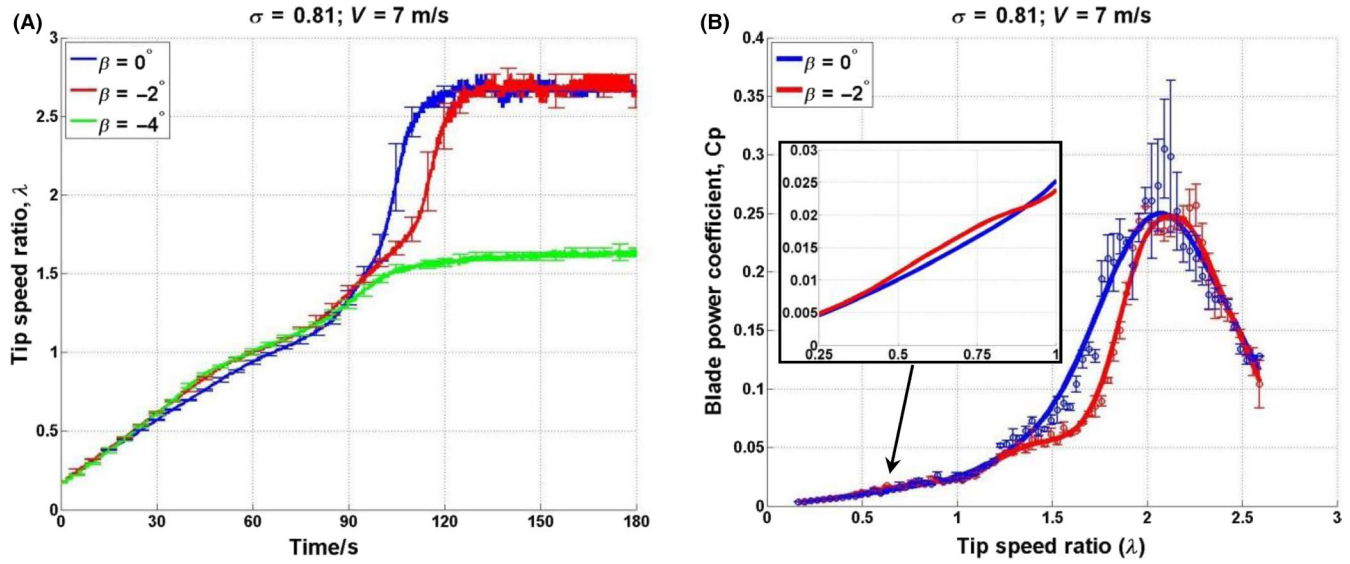

FIGURE 15 Blade pitch effects on turbine performance at $\sigma = 0.81$ and $V = 7$ m/s. A, Self-starting, time-varying results. B, $C_p \sim \lambda$ curve

This varying blade Reynolds number inevitably makes the problem more complex, and more studies need be performed to analyze the dynamic effect of blade surface roughness on turbine performance.

4.4 | Turbine performance with different blade spans

The blade aspect ratio ($AR = S/c$) plays a key role in determining the performance of a three-dimensional blade. It is generally acknowledged that the tip loss phenomenon will degrade the blade performance and this is worsened if the AR is low. The blade tested here was the NACA0021 and previous analytical studies[44] of turbines with NACA0018 blades at similar Reynolds range indicate an aspect ratio $AR > 5.7$ (keeping c the same) is a requisite for a turbine achieving self-starting at $V = 7$ m/s. Therefore, experimental measurements were performed in the present study to test that conclusion with blade spans of $S = 600$ mm and $S = 700$ mm (resulting in an aspect ratios of 6 and 7, respectively), the latter already having been shown to self-start. It should be noted that the blade chord length was kept constant at $c = 100$ mm.

It is surprising to find that by reducing the blade aspect ratio by only 14% to $AR = 6$, the turbine failed to self-start under any of the investigated solidities despite lying above the $AR > 5.7$ threshold. Examples at $V = 7$ m/s are illustrated in Figure 20. As can be seen, the turbine with $AR = 6$ accelerates much more slowly from the start even at the highest solidity of $\sigma = 1.0$ and the turbine produces very limited net positive torque thus achieving a maximum tip speed ratio of only $\lambda = 0.85$. It seems that after removing 100 mm (14%) of

blade span, the reduced aerodynamic torque was insufficient to overcome system resistance thus preventing start-up. For the delicate process of H-Darrieus self-starting, any small loss of useful torque might be fatal to the turbine.

The tests were repeated by using the DU06W200 blades which yielded the same conclusion, that a turbine cannot self-start under any test condition with the blade aspect ratio of $AR = 6$. Therefore, from these results, it might be expected that increasing the blade span of any VAWT would lead to better starting performance as a consequence of increasing the marginal difference between the aerodynamic torque and the system resistance including blade tip loss.

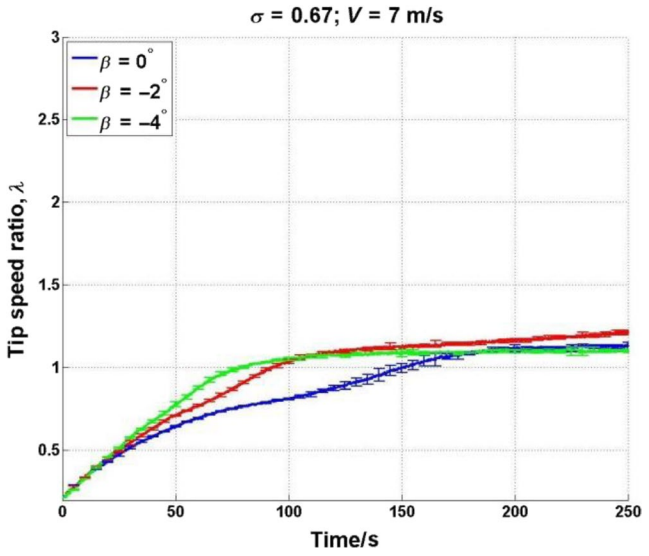

FIGURE 16 Blade pitch effects on turbine performance at $\sigma = 0.67$ and $V = 7$ m/s. Self-starting, time-varying results

5 | CONCLUSIONS

A three-bladed H-Darrieus wind turbine was experimentally tested to investigate the effect of independent design parameters including blade profile, surface roughness, pitch angle, aspect ratio, and turbine solidity on turbine performance. Three typical blades (NACA0021, DU06W200, and NACA4415) were tested under three turbine solidities of $\sigma = 0.67$ (low), $\sigma = 0.81$ (middle), and $\sigma = 1.0$ (high). Blade pitch angles of $\beta = 0°$, $\beta = -2°$ and $\beta \geq -4°$ were also investigated. Moreover, blades with wooden surface (rough) and blades coated with thin aluminum tape (smooth) were tested and compared. Finally, the blade aspect ratio was modified by changing the blade span and two aspect ratios of $AR = 7$ and $AR = 6$ were examined.

Turbine time-varying, self-starting behavior has been presented together with overall $C_p \sim \lambda$ performance data. This study provides comprehensive experimental data for studying and designing a small-scale (low Reynolds number) H-Darrieus wind turbine. Special attention was paid to the turbine behavior and performance at low tip speed ratios in order to gain greater understanding of the factors that influence the ability of a turbine to self-start and consequently to provide clear guidelines for the design of self-starting H-Darrieus wind turbines. Based on the experimental results, important conclusions can be drawn as follows:

- Of the three different blade profiles that were examined, the DU06W200 profile demonstrates the highest peak C_p. However, turbine self-starting time is improved by using the NACA0021 profile since it generates more power at low λ. The cambered NACA4415 profile which has been recommended by previous researchers failed to self-start

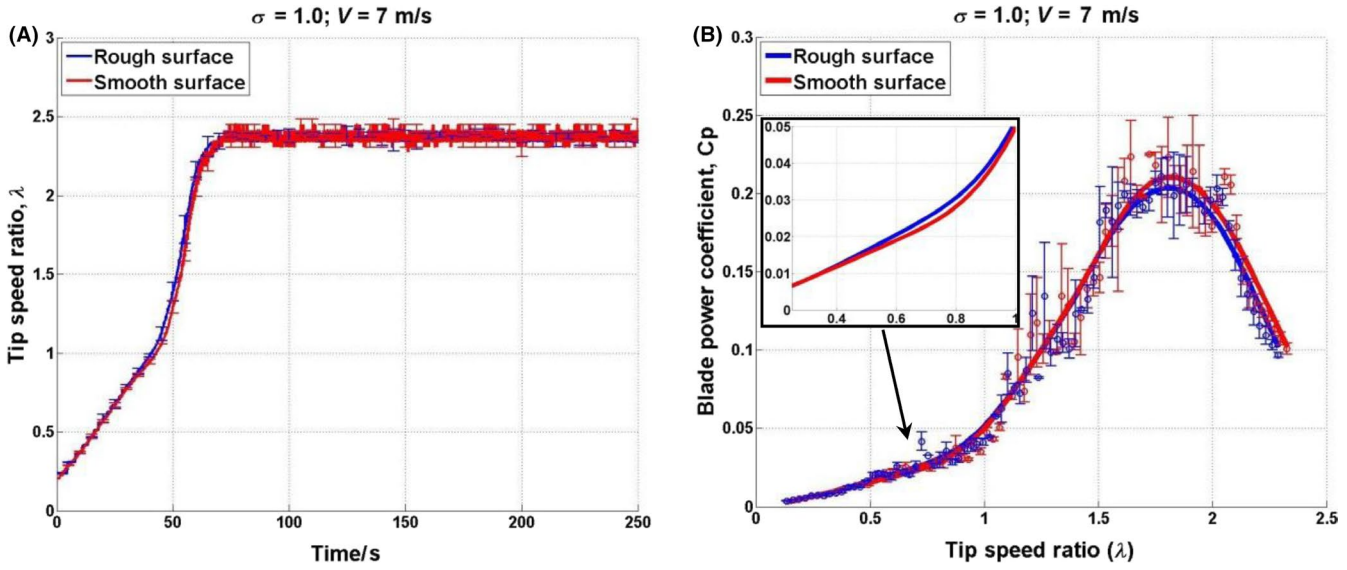

FIGURE 17 Blade surface roughness effect on turbine performance at $\sigma = 1.0$ and $V = 7$ m/s. A, Self-starting, time-varying results. B, $C_p \sim \lambda$ curve

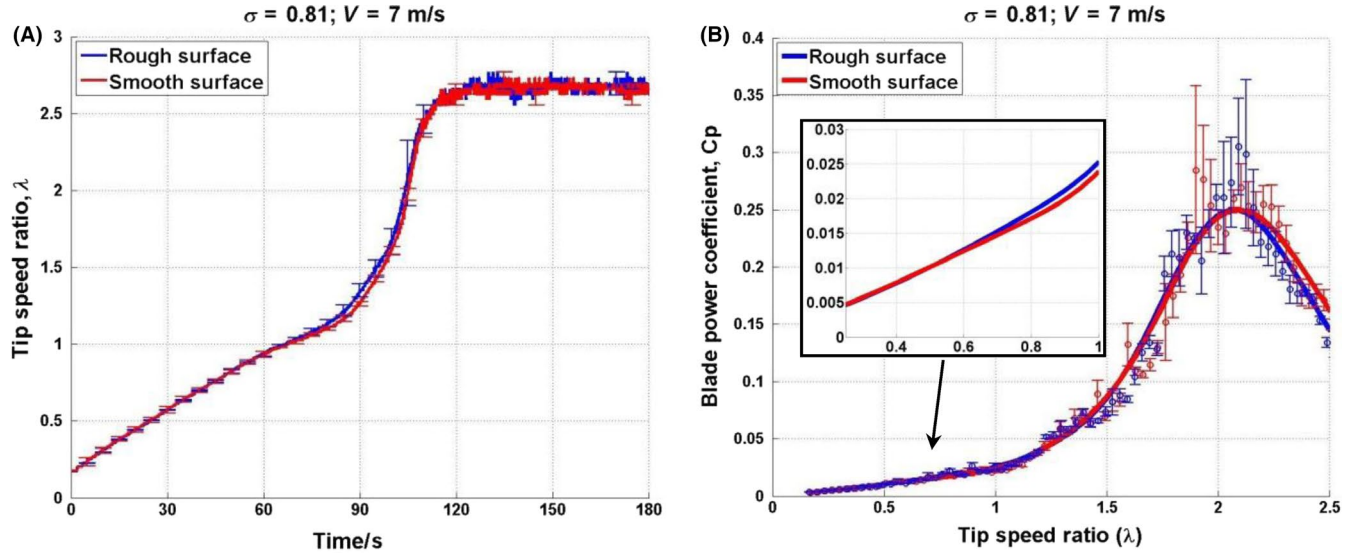

FIGURE 18 Blade surface roughness effect on turbine performance at $\sigma = 0.81$ and $V = 7$ m/s. A, Self-starting, time-varying results. B, $C_p \sim \lambda$ curve

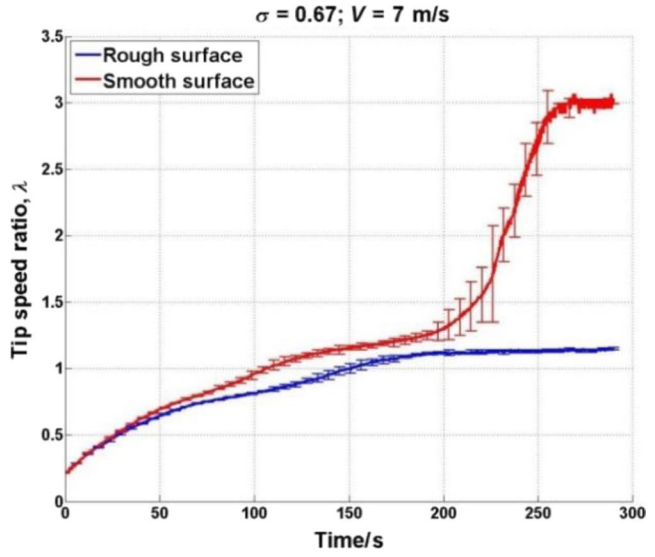

FIGURE 19 Blade surface roughness effect on turbine performance at $\sigma = 0.67$, $V = 7$ m/s

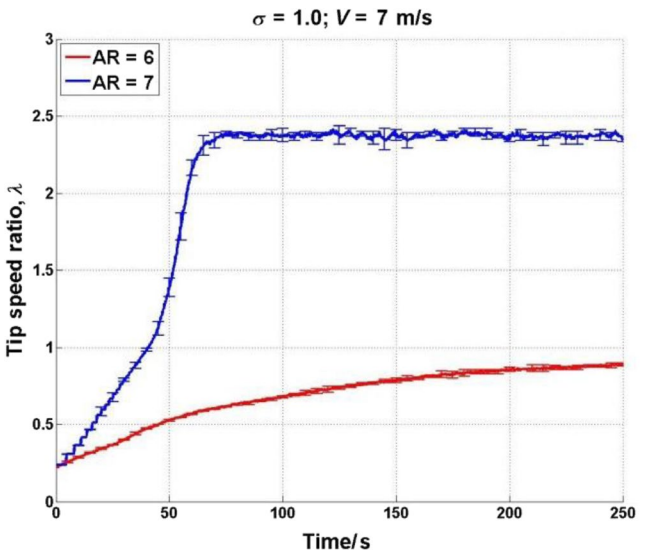

FIGURE 20 Self-starting time-varying results for turbine with different blade aspect ratios at $\sigma = 1.0$

under any test conditions. Thus, the traditional symmetrical NACA series with large thickness still presents a simple but effective choice of blade geometry achieving a good compromise between good starting performance and adequate peak power operation.

- Turbines with high solidity ($\sigma \geq 0.81$) are able to self-start faster than turbines with low solidity due to the increased flow blockage. However, this is achieved at the expense of lower peak power output. Therefore, a balance must be struck between stronger self-starting capability and larger peak power output.
- Small, negative blade pitch ($\beta \geq -2°$) can delay the blade stall in the upwind region resulting in more torque generated at low λ. Although the blade performance at relatively high λ is slightly degraded, it is thought blades with a small negatively pitched angle can help the turbine pass through the "dead band"/plateau stage more easily, which occurs at low tip speed ratios.
- The blade surface roughness can affect the turbine performance. Rough blades tend to increase the turbine performance at low tip speed ratios due to an earlier laminar to turbulent boundary layer transition, which delays the blade stall. In contrast, smooth blades perform better at high tip speed ratios resulting from lower skin friction. An exceptional case is observed for a turbine solidity of $\sigma = 0.67$, where the turbine with smooth blades successfully enables

the turbine to self-start while the rough-bladed turbine fails to self-start. One possible explanation is at this low solidity (low blockage) the benefit from the delayed stall of a rough surface becomes limited and cannot make up for the loss from the increased skin friction drag.

- The present study demonstrates that by decreasing the blade span from $S = 700\,\text{mm}$ to $S = 600\,\text{mm}$ (14% reduction), the turbine self-starting capability is considerably decreased. Larger blade span resulting in larger blade aspect ratio is helpful to reduce the blade's 3D effects, enabling faster turbine self-starting and increasing the marginal difference between the aerodynamic torque and the system resistance including blade tip loss.

ACKNOWLEDGMENT

The authors would like to thank the technical staff in the Department of Engineering of Durham University for their help in setting up the wind turbine. This work was funded by the Sichuan Science and Technology Program (No. 2018JY0595).

NOMENCLATURE

SYMBOLS

A	turbine frontal area, m^2
AR	blade aspect ratio
c	chord length, mm
C_T	torque coefficient
C_p	power coefficient
d	diameter of the central shaft mm
f	frequency, Hz
I_s	system moment of inertia including blades, kg m^2
I_{rig}	system moment of inertia excluding blades, kg m^2
m	weight, kg
n	number of blade
p	smoothing parameter
R	turbine radius, mm
S	blade span, mm
S_a	arithmetic mean height, μm
S_q	root mean squared height, μm
t	reading time, s
T_B	blade torque, N m
T_{res}	system resistant torque excluding the blades, N m
V	upstream wind speed, m/s

GREEK SYMBOLS

λ	tip speed ratio
β	pitch angle, °
σ	turbine solidity
ξ	angular acceleration, rad/s^2
ξ'	angular deceleration, rad/s^2
ω	rotational speed, rad/s
ρ	air density, kg/m^3
δ	shaft-to-turbine diameter ratio

ABBREVIATIONS

CFD	computational fluid dynamics
DMST	double-multiple streamtube model
HAWT	horizontal axis wind turbine
PIV	particle image velocimetry
Re	Reynolds number
VAWT	vertical axis wind turbine

ORCID

Longhuan Du https://orcid.org/0000-0001-7318-1250

REFERENCES

1. Ahmadi-Baloutaki M, Carriveau R, Ting D. A wind tunnel study on the aerodynamic interaction of vertical axis wind turbines in array configurations. *Renewable Energy*. 2016;96:904-913.
2. Bertenyi T, Wickins C, Mcintosh SC. Enhanced energy capture through gust-tracking in the urban wind environment. In: *48th AIAA Aerospace Sciences Meeting Including the New Horizons Forum and Aerospace Exposition*. Orlando, Florida, USA, 4–7 January 2010. Paper No. AIAA 2010–1376.
3. Edwards JM, Danao LA, Novel H. Experimental power curve determination and computational methods for the performance analysis of vertical axis wind turbines. *J Sol Energy Eng*. 2012;134(3):031008.
4. Jin X, Zhao G, Gao K, Ju W. Darrieus vertical axis wind turbine: basic research methods. *Renew Sustain Energy Rev*. 2015;42:212-225.
5. Zanforlin S. Advantages of vertical axis tidal turbines set in close proximity: a comparative CFD investigation in the English Channel. *Ocean Eng*. 2018;156:358-372.
6. Dominy RG, Lunt P, Bickerdyke A, et al. Self-starting capability of a Darrieus turbine. *Proc Inst Mech Eng, Part A: J Power Energy*. 2012;221(1):111-120.
7. Saeidi D, Sedaghat A, Alamdari P, Alemrajabi AA. Aerodynamic design and economical evaluation of site specific small vertical axis wind turbines. *Appl Energy*. 2013;101(1):765-775.
8. Svorcan J, Stupar S, Komarov D, Peković O, Kostić I. Aerodynamic design and analysis of a small-scale vertical axis wind turbine. *J Mech Sci Technol*. 2013;27(8):2367-2373.
9. De Tavernier D, Simao Ferreira C, van Bussel G. Airfoil optimisation for vertical-axis wind turbines with variable pitch. *Wind Energy*. 2019;22:547-562.
10. Dumitrescu H. Low-frequency noise prediction of vertical axis wind turbines. *Proc Romanian Acad, Ser A*. 2010;11:47-54.
11. Hand B, Cashman A. Conceptual design of a large-scale floating offshore vertical axis wind turbine. *Energy Procedia*. 2017;142:83-88.

12. Hand B, Cashman A. Aerodynamic modeling methods for a large-scale vertical axis wind turbine: a comparative study. *Renewable Energy*. 2018;129:12-31.
13. Untaroiu A, Wood HG, Allaire PE, Ribando RJ. Investigation of self-starting capability of vertical axis wind turbines using a computational fluid dynamics approach. *J Sol Energy Eng*. 2011;133(4):041010.
14. Arab A, Javadi M, Anbarsooz M, Moghiman M. A numerical study on the aerodynamic performance and the selfstarting characteristics of a Darrieus wind turbine considering its moment of inertia. *Renewable Energy*. 2017;107:298-311.
15. Howell R, Qin N, Edwards J, Durrani N. Wind tunnel and numerical study of a small vertical axis wind turbine. *Renewable Energy*. 2010;35(2):412-422.
16. Danao LA, Edwards J, Eboibi O, Howell R. A numerical investigation into the influence of unsteady wind on the performance and aerodynamics of a vertical axis wind turbine. *Appl Energy*. 2014;116:111-124.
17. Zhu H, Hao W, Li C, Ding Q. Numerical study of effect of solidity on vertical axis wind turbine with Gurney flap. *Wind Eng Ind Aerodynam*. 2019;186:17-31.
18. Rezaeiha A, Montazeri H, Blocken B. Towards optimal aerodynamic design of vertical axis wind turbines: impact of solidity and number of blades. *Energy*. 2018;165:1129-1148.
19. Rezaeiha A, Montazeri H, Blocken B. Characterization of aerodynamic performance of vertical axis wind turbines: impact of operational parameters. *Energy Convers Manag*. 2018;169:45-77.
20. Wang Z, Zhuang M. Leading-edge serrations for performance improvement on a vertical-axis wind turbine at low tip-speed-ratios. *Appl Energy*. 2017;208:1184-1197.
21. Wang Z, Wang Y, Zhuang M. Improvement of the aerodynamic performance of vertical axis wind turbines with leading-edge serrations and helical blades using CFD and Taguchi method. *Energy Convers Manag*. 2018;177:107-121.
22. Zanforlin S, Deluca S. Effects of the Reynolds number and the tip losses on the optimal aspect ratio of straight-bladed Vertical Axis Wind Turbines. *Energy*. 2018;148:179-195.
23. Mazarbhuiya H, Biswas A, Sharma KK. Performance investigations of modified asymmetric blade H-Darrieus VAWT rotors. *J Renewable Sustain Energy*. 2018;10(3):033302.
24. Bianchini A, Balduzzi F, Ferrara G, et al. Detailed analysis of the wake structure of a straight-blade H-Darrieus wind turbine by means of wind tunnel experiments and computational fluid dynamics simulations. *J Eng Gas Turbine Power*. 2018;140(3):032604.
25. Weber J, Becker S, Scheit C, Grabinger J, Kaltenbacher M. Aeroacoustics of Darrieus wind turbine. *Aeroacoustics*. 2015;14:883-902.
26. Battisti L, Persico G, Dossena V, et al. Experimental benchmark data for H-shaped and troposkien VAWT architectures. *Renewable Energy*. 2018;125:425-444.
27. Miller MA, Duvvuri S, Brownstein I, Lee M, Dabiri JO, Hultmark M. Vertical-axis wind turbine experiments at full dynamic similarity. *Fluid Mecha*. 2018;844:707-720.
28. Parker CM, Leftwich MC. The effect of tip speed ratio on a vertical axis wind turbine at high Reynolds numbers. *Exp Fluids*. 2016;57(5):74.
29. Tescione G, Ragni D, He C, Simão Ferreira CJ, van Bussel G. Near wake flow analysis of a vertical axis wind turbine by stereoscopic particle image velocimetry. *Renewable Energy*. 2014;70:47-61.
30. Rolin VF-C, Porté-Agel F. Experimental investigation of vertical-axis wind-turbine wakes in boundary layer flow. *Renewable Energy*. 2018;118:1-13.
31. Buchner A-J, Lohry MW, Martinelli L, Soria J, Smits AJ. Dynamic stall in vertical axis wind turbines: comparing experiments and computations. *Wind Eng Ind Aerodynam*. 2015;146:163-171.
32. Hill N, Dominy RG, Ingram G, et al. Darrieus turbines: the physics of self-starting. *Proc Inst Mech Eng, Part A: J Power Energy*. 2008;223:21-29.
33. Castelli M, Englaro A, Benini E. The Darrieus wind turbine: proposal for a new performance prediction model based on CFD. *J Energy*. 2011;36(8):4919-4934.
34. Rossetti A, Pavesi G. Comparison of different numerical approaches to the study of the H-Darrieus turbines start-up. *J Renewable Energy*. 2013;50:7-19.
35. Claessens M. *The Design and Testing of Airfoils for Application in Small Vertical Axis Wind Turbines*. Master thesis, Faculty of Aerospace Engineering, Delft University of Technology, Netherlands; 2006.
36. Kirke BK, Lazauskas L. Enhancing the performance of a vertical axis wind turbine using a simple variable pitch system. *Wind Eng*. 1991;15(4):187-195.
37. Klimas P, Worstell M. *Effects of Blade Preset Pitch/Offset on Curved-blade Darrieus Vertical Axis Wind Turbine Performance*. Technical Report No. SAND81-1762, Sandia National Laboratories, USA: 1981.
38. Du L. *Numerical and Experimental Investigations of Darrieus Wind Turbine Start-up and Operation*. PhD Thesis, University of Durham, UK; 2016.
39. ZETA-20. http://www.zeta-inst.com/products/true-color-3D-optical-profiler. Accessed June 24, 2019.
40. Rezaeiha A, Kalkman I, Montazeri H, Blocken B. Effect of the shaft on the aerodynamic performance of urban vertical axis wind turbines. *Energy Convers Manage*. 2017;149:616-630.
41. Du L, Berson A, Dominy RG. The prediction of the performance and starting capability of H-Darrieus wind turbines. *ASME Turbo Expo*. Montreal, Canada, 15-19 June 2015, Paper No. GT2015-4221.
42. Du L, Imgram G, Dominy RG. Time-accurate blade surface static pressure behaviour on a rotating H-Darrieus wind turbine. *Wind Energy*. 2019;22(4):563-575.
43. AshwillTD. *Measured Data for the Sandia 34 m Vertical Axis Wind Turbine*. Sandia Laboratories, SAND91-2228; 1992.
44. Small WS. *Wind Turbine Starting Behaviour*. Dissertation, School of Engineering and Computing Science, University of Durham, UK; 2012.

How to cite this article: Du L, Ingram G, Dominy RG. Experimental study of the effects of turbine solidity, blade profile, pitch angle, surface roughness, and aspect ratio on the H-Darrieus wind turbine self-starting and overall performance. *Energy Sci Eng*. 2019;00:1–16. https://doi.org/10.1002/ese3.430